THE ASTRONOMICAL JOURNAL VOLUME 106, NUMBER 6 DECEMBER 1993

SUBARCMINUTE RESOLUTION IMAGING OF RADIO SOURCES AT 74 MHz WITH THE VERY LARGE ARRAY

N. E. KASSIM

Code 7215, Remote Sensing Division, Naval Research Laboratory, Washington, DC 20375-5351
Electronic mail: kassim@rira.nrl.navy.mil

R. A. PERLEY

National Radio Astronomy Observatory, P.O. Box 0, Socorro, New Mexico 87801
Electronic mail: rperley@nrao.edu

W. C. ERICKSON

Physics Department, University of Tasmania, Hobart, Tasmania 7001, Australia
Electronic mail: berickson@physvax.utas.oz.au@munnari.oz.au

K. S. DWARAKANATH[1]

National Radio Astronomy Observatory, P.O. Box 0, Socorro, New Mexico 87801
Electronic mail: kdwaraka@nrao.edu

ABSTRACT

A new observing system operating at 74 MHz and providing an angular resolution of 20″ is currently being tested at the VLA. The system comprises a prime-focus dipole feed and amplifier installed on eight of the VLA's 25 m antennas. Although the system is of low efficiency, it works well for imaging strong sources ($S \sim \geqslant 200$ Jy) on long baselines (>5 km) since self-calibration has sufficient signal to noise to remove phase errors on the short time scales (~ 10 s) characteristic of ionospheric variations. We present maps of a few strong, well known radio sources imaged in most cases with unprecedented angular resolution. For weaker sources, the ionospheric phase variations do not allow the increased integration times required for successful self-calibration. In order to overcome this, we have developed a procedure of dual-frequency ionospheric phase referencing utilizing simultaneous observations at 74 and 330 MHz to "unwind" the effects of the ionosphere before self-calibration. We will discuss the procedure, which should be applicable to any future low frequency (<100 MHz), long baseline (>5 km), ground-based interferometer which can obtain simultaneous, higher frequency measurements, and show examples of its application.

1. INTRODUCTION

Improved angular resolution is often the critical driver for the evolution of astronomical telescopes of all types. In the radio regime, the techniques of radio interferometry and earth-rotation aperture synthesis have enjoyed wide success now for decades. As a result, many of today's leading radio astronomical observatories employ sophisticated, multielement synthesis instruments which allow full-field, diffraction limited imaging of astronomical radio sources.

Ironically, while most advancements in radio interferometric techniques were pioneered at the longest wavelengths, there are today no more than a few instruments which employ these techniques for high resolution observations below 400 MHz. And below 100 MHz, there now exist no large aperture (>5 km), low frequency synthesis imaging telescopes, despite the many interesting astrophysical questions which can be addressed only by low frequency, high angular resolution observations. These questions span virtually all areas of astrophysics, including Galactic, extragalactic, solar system, and planetary astrophysics (see, e.g., Kassim & Weiler 1990, and references therein for a review). An important exception to this trend is India's Giant Meter Wavelength Radio Telescope (GMRT) designed for operation between $\sim$38–1400 MHz. The GMRT is expected to become operational by 1995 (Swarup 1993).

The fundamental issue which has prevented the construction of such an instrument in the past has been the corrupting influence of the earth's ionosphere on the measurement of the visibility phase of radio sources on baselines longer than a few km. This has made routine imaging with long baseline, low frequency systems difficult to impossible in the past. Thus, even though the required resources remain significantly lower than those for comparable higher frequency systems, the funding for the construction of such an instrument is contingent on solving the calibration and imaging problems.

The modern techniques of self-calibration, which have been developed to solve similar, although less severe prob-

[1]On leave from Raman Research Institute, Bangalore 560 080, India.

 0004-6256/93/106(6)/2218/11/$0.90

lems in calibration and imaging at centimeter wavelengths, would appear to offer some hope of removing the ionospheric corruption which has so severely restricted imaging at low frequencies. In order to test the application of these, and other solutions to the fundamental restrictions imposed by the ionosphere, the NRAO has constructed a new observing system at the VLA[2] operating in the Radio Astronomy 73.8 MHz band. It is a modest implementation of a bolder, stand-alone system first proposed by Perley & Erickson (1984). A description of this new system is given in Sec. 2.

Calibration is one of two crucial challenges facing long baseline, low frequency systems, and we discuss the procedures we have developed to overcome the effects of radio frequency interference (RFI) and ionospheric phase variation in Secs. 3 and 4, respectively. While we can employ self-calibration for imaging strong sources, we have also developed a method of dual frequency ionospheric phase referencing for imaging weaker sources. It is a powerful technique which utilizes the VLA's ability to obtain data simultaneously at two frequencies. The other great challenge is imaging, and although we discuss a few related issues in Sec. 4, we do not address this subject in any detail here. This topic will be investigated further in future papers.

Our observations of a few prominent radio sources are described in Sec. 5, and some of our first images are presented in Sec. 6. In Sec. 7 we summarize the capabilities of the present system, and the means by which the techniques we have developed can be implemented in future instruments.

2. SYSTEM DESCRIPTION

2.1 Hardware

The new low frequency system utilizes eight of the VLA's 25 m antennas which have been equipped with 74 MHz prime-focus, cross-dipole feeds. These feeds use the subreflector as a crude backplane. The aperture efficiency of each antenna is $\sim$25% at 74 MHz (corresponding to an effective area of $\sim$125 m^2 per dish) yielding an overall collecting area of $\sim$1000 m^2 for the present system. The poor aperture efficiency is primarily due to the interaction of the 74 MHz feeds with the subreflector support legs and the crudeness of the small subreflectors as 74 MHz backplanes; thus the dishes are poorly illuminated and the primary beams have high sidelobes, resulting in poor rejection of strong sources outside the primary field of view.

The 74 MHz signal is amplified by transistor amplifiers, then injected into the standard VLA electronics system through an alternate port on the 330 MHz converter chassis. From this point on, the existing VLA waveguide transmission system, correlator, and computer systems are utilized, thus limiting the cost to approximately \$4 K per antenna.

[2]The VLA is a facility of the National Radio Astronomy Observatory operated by Associated Universities, Inc., under a cooperative agreement with the National Science Foundation.

2.2 Sensitivity

The system sensitivity due to thermal noise is estimated from the standard radiometer equation:

$$S_{\rm rms}({\rm mJy}) = K[(N)(N-1)n\,\Delta t\,\Delta\nu]^{-1/2}, \quad (1)$$

where N is the number of available antennas, n is the number of IF channels, Δt and $\Delta\nu$ are the integration time in hours and the available bandwidth per IF channel in MHz, respectively. K is a system parameter defined as

$$K = 0.082 T_{\rm sys}/\eta \quad (2)$$

with the system temperature, $T_{\rm sys}$, in degrees Kelvin (K) and η the aperture efficiency of each element. For most systems operating below a few hundred MHz, $T_{\rm sys}$ ($T_{\rm sys} = T_{\rm sky} + T_{\rm rec}$) is dominated by $T_{\rm sky}$ since the nonthermal background radiation from the Galaxy usually far exceeds the receiver noise, $T_{\rm rec}$. $T_{\rm sys}$ as measured with our system varies with position on the sky over the range $\sim$1000–6000 K.[3] A representative value is $T_{\rm sys} \approx 2000$ K, which with 1 IF, 8 antennas, $\eta = 25\%$, and an effective bandwidth of $\approx$1 MHz (as is typically used) corresponds to an effective sensitivity in 10 minutes integration, based on thermal noise considerations alone, of a few hundred mJy at 74 MHz.

In practice, the presence of confusion noise lowers the effective sensitivity considerably. This is especially true for this system since the primary beam of the VLA antennas at 74 MHz is large ($\sim$13 degrees FWHP) with very high sidelobes. Thus, fluctuations in the output due to the correlated signals from the sidelobe response to high flux density sources outside the primary field-of-view degrade the effective sensitivity. The magnitude of this effect, which depends strongly on many parameters such as baseline length, sky position, bandwidth, time averaging and the primary beam shape is difficult to quantify. Rough estimates (Perley and Erickson 1984) indicate that for the bandwidths being used, the confusion noise will significantly exceed thermal noise. A quantitative estimate has been obtained from the first images.

The images presented in Sec. 6 usually reached an effective rms noise level of $\sim$1 Jy beam^{-1}. This was achieved typically with seven antennas, an effective bandwidth of 0.75 MHz, and a total integration time of approximately 50 min. Equations (1) and (2), with these parameters, then predict a thermal noise level lower than that achieved by factors of $\sim$3–4, indicating the domination of confusion. Since the confusion noise is a strong function of (u,v) coverage, we are optimistic that the level will be greatly reduced with more antennas.

For a small subset of the very strongest sources (e.g., Cyg A, Cas A) the effective noise levels are dynamic range

[3]$T_{\rm sky}$ can be estimated by comparison with the all-sky radio maps at 85 MHz (Yates 1968) and at 150 MHz (Landecker & Wielebinski 1970) or from more recent surveys at 34 MHz (Dwarakanath & Udaya Shankar 1990) and at 408 MHz (Haslam *et al.* 1982). It varies from $\sim$900 K at the Galactic pole to over 9000 K in a small region near the Galactic Center. But for this system, with its large primary beam and extensive sidelobes, $T_{\rm sys}$ varies over a smaller range.

limited. In such cases the effective noise levels are approximately 20 dB below the brightest peaks in the map, and is comparable to the dynamic ranges obtained at other frequencies with similar quantities of data. This is a very reasonable value given the complexity of the sources and the small amount of data presently available for imaging.

3. RADIO FREQUENCY INTERFERENCE (RFI)

3.1 Externally Generated RFI

Radio Frequency Interference (RFI) can be a major problem at low frequencies. For the current system we employ a bandwidth of $\approx$0.75–1.5 MHz centered on the 73.0 to 74.6 MHz Radio Astronomy allocation. We find little external RFI within this band, but elimination of a strong 71.75 MHz TV sound carrier requires an RF filter with good adjacent band rejection. Since external RFI is often significantly higher during "normal working hours" than during the night time and on weekends, observations are scheduled appropriately when possible.

Intermittent RFI occasionally affects the 330 MHz data. It can usually be excised using standard editing procedures.

3.2 Internally Generated RFI

By internal RFI, we mean signals generated by the antenna electronics, or by other equipment located at the VLA site. Two forms of such internally generated RFI are relevant to our system. The first is harmonics of signals generated within the fringe rotation electronics located in each VLA antenna. These harmonics are at multiples of 5 and 12.5 MHz, are extremely strong and phase coherent, and must be suppressed by shielding the electronics racks housing the fringe rotation electronics. A modest program to do this is underway, and twelve antennas are currently shielded. The presence of these harmonics forces narrow bandwidths (typically 3.125 MHz) to be employed at *P* band ($\sim$327–333 MHz) but imposes no restrictions on the 4-band (74 MHz) system, since the front-end filters are 1.6 MHz, centered at 73.8 MHz.

More important to 74 MHz observations are harmonics of 100 kHz generated by the digital data communications system in each antenna. These signals were originally phase locked to the master oscillator and were all phase coherent. Thus, radiated signals from each electronics rack were received at that antenna's feed, and were coherently detected in the correlator. The problem was severe since the correlated power via this mechanism was several orders of magnitude greater than that from the strongest astronomical radio source. Since these harmonics originate from many different locales in the antenna, shielding was not a practical solution. This problem has been neatly eliminated by rendering these signals incoherent, a solution proposed and implemented by Durga Bagri.

The only serious remaining problem is caused by those signals which cross couple between antennas, i.e., signals generated by the electronics in one antenna that are radiated to it, and other antennas. These signals show up as narrow-band interference spikes in the cross-power spectra. Fortunately, these cross-radiated couplings are not strong, and can be easily eliminated by observing in a spectral-line mode with high spectral resolution and flagging the affected channels.

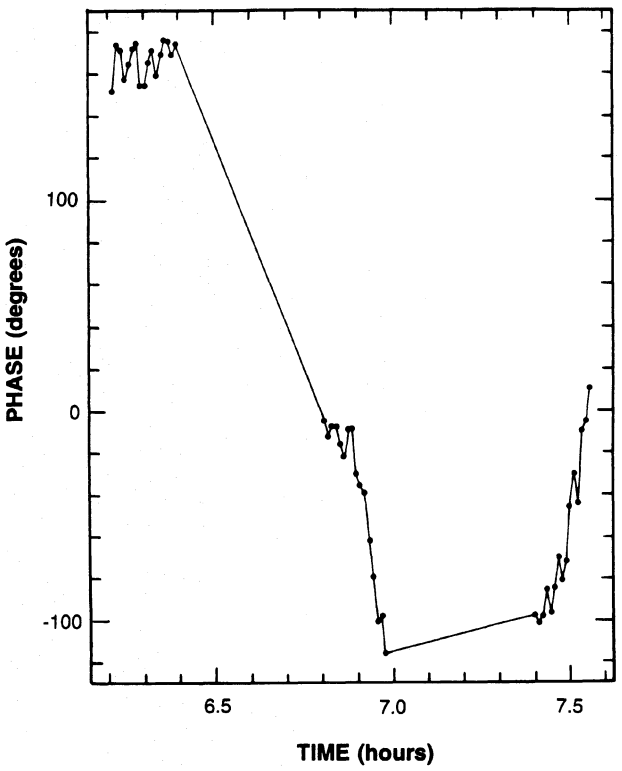

FIG. 1. Plot of visibility phase (in degrees) vs time (in hours) for three 10 min "snapshot" observations of Virgo A (3C274) at 74 MHz on a baseline of $\sim$10 km length. The source is located near the field center and the samples are at 30 s intervals. In the absence of ionospheric effects, the phase variations within each snapshot would be negligible ($<5°$).

Finally, we note that there is often some additional "local RFI" generated by various equipment at the VLA site (e.g., telephone modems). This interference is usually easily recognized and edited, but it cannot be ignored and does add additional work time to the data reduction process.

4. CALIBRATION

4.1 Self-calibration Imaging of Strong Sources

Phase calibration is the most formidable challenge to observations with the 74 MHz system. Amplitude calibration can be based on observations of isolated, small diameter sources such as 3C123 ($S_{73.8}\approx$400 Jy), following well established procedures. However, such observations cannot be used for phase calibration of target sources, since differential phase offsets between antennas introduced by the ionosphere change rapidly as a function of time and position on the sky. For example, even on medium baselines ($\approx$5–10 km), phases can drift at rates of up to 1 degree second^{-1} at 74 MHz.

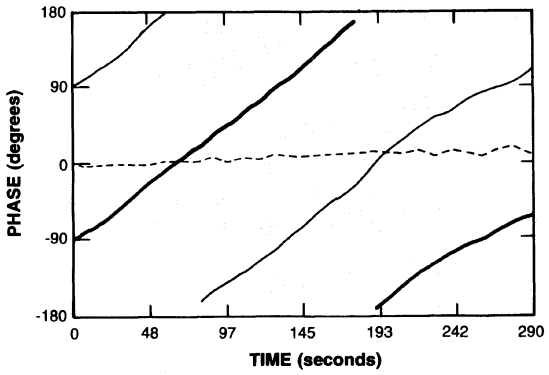

FIG. 2. Plot of visibility phase (in degrees) vs time (in seconds) on a ~15 km baseline for a point source located at the phase center. The thick solid line is the phase measured at 74 MHz and plotted at an arbitrary starting phase of −90°. The ~360° phase wind which occurs during the ~5 min snapshot observations is due to the ionosphere. The thin solid line is the same plot for the 330 MHz visibility phase after it has been multiplied by the ratio of the frequencies (330/74), and it has been plotted at an arbitrary starting phase of +90°. The dashed line represents the difference between the two and illustrates how well the "scaled" 330 MHz phase tracks the ionospheric phase variations at 74 MHz.

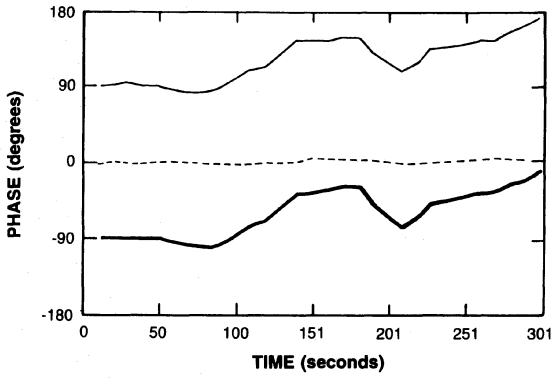

FIG. 3. Same as in Fig. 2 for a case where the ionospheric phase variations are less smooth.

To illustrate this, Fig. 1 shows a plot of phase as a function of time for three 10 min "snapshot" observations of Virgo A (3C274) on a baseline of ~10 km length. The samples are at 30 s intervals. In the absence of ionospheric effects, little drift ($\ll\pi$ radians per snapshot) in visibility phase should occur over a period of many hours for a source such as this which is approximately symmetrically positioned about the phase center. Instead, significantly different phase signatures result from each snapshot. During the first snapshot the phase jitters but remains roughly constant, during the second it decreases significantly ($\approx -100°$), and during the third it increases significantly ($\approx +100°$). However, the changes are fairly smooth as a function of time and relatively small ($\approx < 5°$) from sample to sample.

Ionospheric effects of the type illustrated in Fig. 1 are so large and unpredictable at 74 MHz that initial phase information is usually completely useless for the purposes of imaging. However, self-calibration procedures [now well advanced for VLA data, see Pearson & Readhead (1984) for a review] are perfectly applicable to 74 MHz data, provided an adequate model of the source and good signal to noise (S/N) are available. In principle, only the absolute position of the source is lost. This technique works when the ionospheric variations are much smaller than a radian within an integration interval (a condition nearly always met in our 10 s default integration interval), the model is a good match to the data (which in practice means the source must dominate the total flux within the beam), and there is sufficient S/N in each sample. Section 6 presents examples of bright sources imaged with the system using this technique. In all cases so far, the 330 MHz map imaged using the VLA in the standard manner produces a quite adequate starting model for the 74 MHz self-calibration algorithm.

In practice we find that the correlated flux density per baseline needs to be 5 to 10 Jy for self-calibration to work reliably on such short time scales. For weaker sources and more severe ionospheric conditions, the S/N within the coherence time of the data is too low for this method to produce a solution. Therefore we have developed a method of dual frequency ionospheric phase referencing to remove the effects of the ionosphere so that longer integration times can be used to increase the S/N ratio, thus permitting self-calibration techniques to be applied to much weaker sources.

4.2 Dual Frequency Ionospheric Phase Referencing

Dual frequency ionospheric phase referencing takes advantage of the VLA's ability to obtain data simultaneously at two frequencies. The basic idea is very straightforward: Since the phase fluctuations at wavelengths longer than about 0.5 m are completely dominated by the ionosphere, knowledge of the fluctuations at one frequency can be used to predict the fluctuations at any other frequency. In our experiments, we have used 330 and 73.8 MHz as the two frequencies. The phase fluctuations at the higher frequency are rarely severe enough to prevent imaging in the standard manner, so an image of the target source made with these data can normally be used to measure the ionospheric phase errors for each antenna as a function of time. These are then extrapolated to 73.8 MHz, and applied to those data. Discussion of the physical properties within the ionosphere which actually give rise to these effects can be found in Perley & Erickson (1984) and Jacobson & Erickson (1992a,b). Details of this procedure are now given.

The ionosphere introduces a path length in addition to the geometric length due to the presence of an ionized medium. This extra path length is given (in MKS units) by

$$\Delta L = -4.5\times 10^{-16}\lambda^2 \int n_e\, dl, \qquad (3)$$

where here n_e is the Total Electron Content or TEC (a measure of column density, typically $\sim 10^{17}$ m^{-2}), λ is the wavelength of observation, and the integral is along the ray path through the ionosphere. Since the phase change in

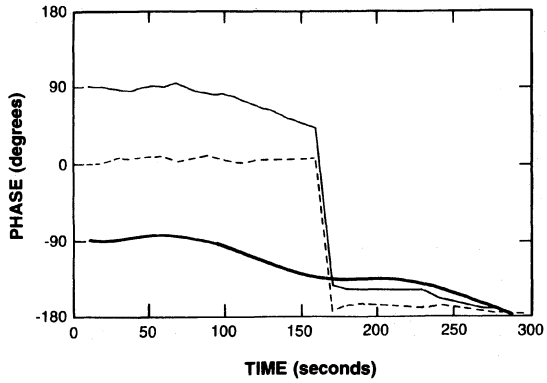

FIG. 4. Same as Figs. 2 and 3, except this figure illustrates the ~165 degree "phase jump" caused by the presence of a 360 degree phase ambiguity discussed in Sec. *4.2*.

radians due to an added path length ΔL is $2\pi\Delta L/\lambda$, we have, from Eq. (3),

$$\Delta\phi = 2\pi\Delta L/\lambda = -4.5\times10^{-16}2\pi\lambda\int n_e\,dl, \qquad (4)$$

where $\Delta\phi$ is the phase difference in radians introduced by the extra path length. At 74 MHz, even though the ionosphere is typically less than 0.01% ionized, the total additional phase introduced can exceed 1000 rad. Certainly the differential electron content between ray paths to different antennas within the VLA is much smaller, but is still significant as illustrated by Fig. 1 above. However, most of the variations we observe are not due to the differential path through a smooth ionosphere, but due to varying horizontal gradients produced by traveling ionospheric waves.

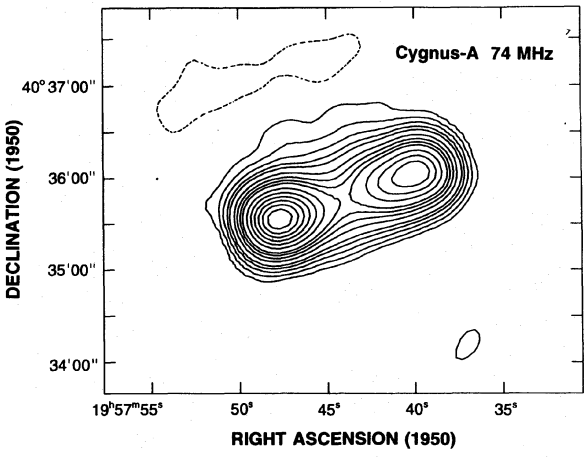

FIG. 5. Contour plot of the radio source Cygnus A at 74 MHz imaged entirely by the dual-frequency phase referencing procedure (see Sec. *4.2*) and using no self-calibration. The peak brightness in the map is ~5000 Jy beam^{-1}, the rms noise on the image is ~50 Jy beam^{-1}, and the angular resolution is ~20″. This image demonstrates the power of phase referencing to remove the rapidly varying ionospheric fluctuations and to restore coherence to the data. Phase referencing has increased the coherence time of the data from < 1 m to > 10 m.

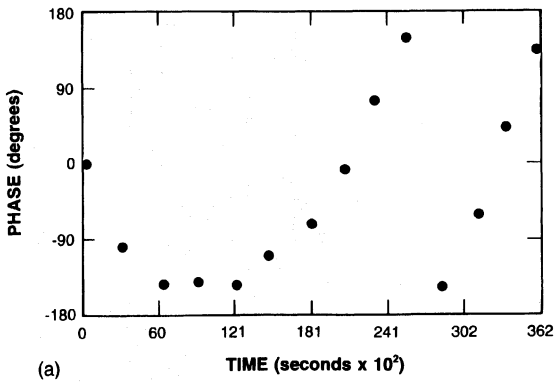

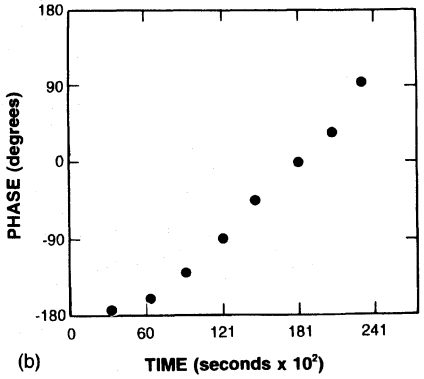

FIG. 6. (a) and (b) Long time scale plots of phase corrected 74 MHz phase (in degrees) vs time (in units of 10^2 s) for a point source at the field center. These phase plots would remain constant as a function of time were it not for the slowly varying effects of ionospheric refraction (see Sec. *4.3.1*). The resulting drift can have rates of up to 1 rad h^{-1} and generally increases in magnitude with increasing baseline length. (a) shows a parabolic shaped drift on an EW baseline, while (b) illustrates a linear shaped drift on a NS baseline. The shape and magnitude of the drift depend on the source/baseline geometry and on the magnitude of the refraction. Techniques are currently being explored to find how best to correct for this effect.

For example, a 1% cyclical variation in ionospheric column density (caused, for example by a Traveling Ionospheric Disturbance) moving at a speed of 100 km h^{-1} with a wavelength of 30 km would cause a 10 rad phase differential between two antennas 30 km apart, with a phase rate of 1 rad min^{-1}. Alternatively, a horizontal gradient in the TEC of 10^{13}/cm^{-2} km would produce 1 rad of phase shift over a 10 km baseline at 74 MHz. Variable gradients of this magnitude, comprising ~0.1% of the TEC per kilometer, are very common (Erickson *et al.* 1988) except under unusually quiet ionospheric conditions. Ionospheric waves have a wide spectrum of spatial and temporal scales (Jacobson & Erickson 1992b) which include the baseline lengths and time periods over which we observe.

At 330 MHz, the self-calibration algorithms have little difficulty in adjusting the antenna-based phases to correct for the ionospheric effects because the ionospheric phase drifts are much smaller, the S/N ratio rather good, and the data are of good quality. An important additional factor is the increased number of antennas (27 at 330 MHz vs 7 or

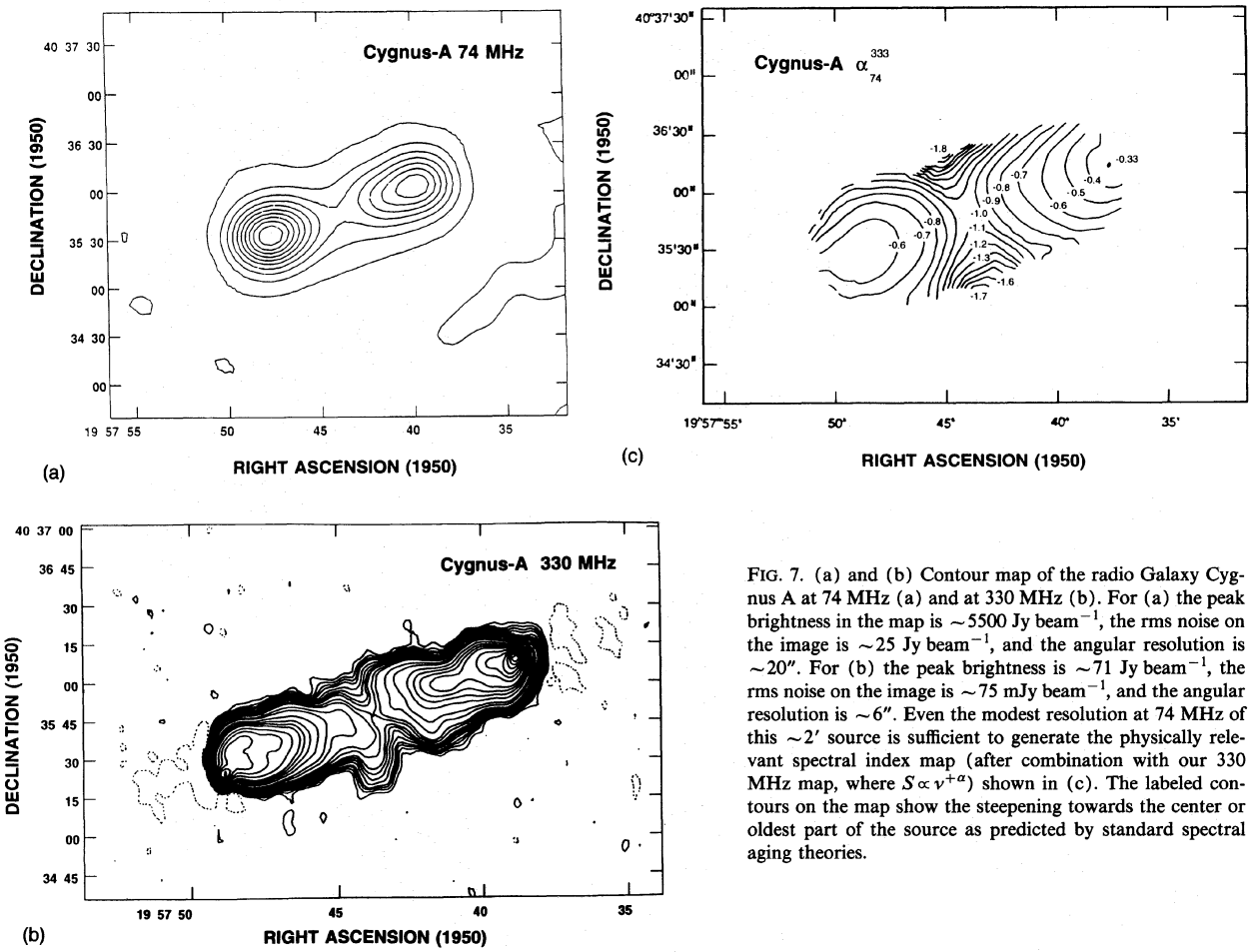

FIG. 7. (a) and (b) Contour map of the radio Galaxy Cygnus A at 74 MHz (a) and at 330 MHz (b). For (a) the peak brightness in the map is $\sim$5500 Jy beam^{-1}, the rms noise on the image is $\sim$25 Jy beam^{-1}, and the angular resolution is $\sim$20″. For (b) the peak brightness is $\sim$71 Jy beam^{-1}, the rms noise on the image is $\sim$75 mJy beam^{-1}, and the angular resolution is $\sim$6″. Even the modest resolution at 74 MHz of this $\sim$2′ source is sufficient to generate the physically relevant spectral index map (after combination with our 330 MHz map, where $S \propto \nu^{+\alpha}$) shown in (c). The labeled contours on the map show the steepening towards the center or oldest part of the source as predicted by standard spectral aging theories.

8 at 74 MHz), allowing much better (u,v) plane coverage and much reduced confusion noise. The resultant 330 MHz antenna phase solutions, properly scaled, are applicable to the simultaneously obtained 74 MHz data. As can be seen from Eq. (4), the ionospheric phase difference between any pair of antennas at the two different frequencies scales linearly with λ.

Because of the linear relation between phase perturbation and observing frequency, it is not necessary to know the "total phase offset" of the 330 MHz data for the method to work. The fluctuations in the phase about this offset scale to the same size fluctuations in the lower frequency phase regardless of the magnitude of the total offset. However, the offset does translate to a different offset at the lower frequency, and this, along with the unique antenna-dependent instrumental phase offset must be calibrated by observing a 74 MHz calibrator.

Calibration of data utilizing the ionospheric phase referencing technique proceeds as follows. A target source is observed simultaneously at both 330 and at 74 MHz. After the source is imaged in the standard manner at 330 MHz, this image is used as a starting model for self-calibration to generate a phase solution which contains the time variable phase offsets introduced by the ionosphere. This solution is then scaled by λ according to Eq. (4) and applied to the 74 MHz data in order to remove the short-term ionospheric effects. In principle these data could then be mapped without self-calibration (e.g., see Fig. 5). However, as a result of residual phase drifts due to ionospheric refraction (see Sec. *4.3.1*), a scan-averaged self-cal is usually required. We find that a 327 MHz model, applied to the 74 MHz data, is sufficient to accomplish this.

Figure 2 shows a plot of visibility phase versus time on a 15 km baseline for a point source which illustrates the technique. In this figure the thick solid line is the phase measured at 74 MHz and plotted at an arbitrary starting phase of $-90°$. Notice that is winds approximately a full cycle over the 5 min shown, rendering self-calibration requiring similar integration times useless. The thin solid line represents the phase measured at 330 MHz multiplied by 330/74, plotted at an arbitrary starting phase of $+90°$, and the dashed line represents the difference between the two. Note that the scaled 330 MHz phase accurately tracks the ionospheric introduced phase wind at 74 MHz. Figure 3 shows a similar plot for a case where the ionospheric phase is not so regular.

An interesting problem surfaces if we are unable to continuously track the 330 MHz phase, as is the case for our cycling, snapshot observations. (In this popular VLA observing mode, sources are only tracked continuously for "snapshots" of $\sim$5–10 min length each.) The best understanding of this comes from considering two, time-

separated observations of an object, between which the 330 MHz phase increases by 360 degrees. The measured phase for both observations will appear to be the same, and the predicted 74 MHz phases will thus also be the same. But because of the (unknown) 360 degree addition, the predicted 74 MHz phase of the second scan will be in error by $360\times(330/74)$ modulo 360 degrees or ~ 165 degrees. Such phase steps are often easy to detect in our phase corrected data but we are still considering how best to handle this problem automatically. Figure 4 illustrates this effect. The simplest solution of observing two, separated frequencies within *P* band cannot be used, since this eliminates simultaneous observation at 4 band. (Alternatively, future observing systems which do not track sources continuously could avoid this problem by choosing a higher frequency which is an integer multiple of the lower frequency.)

Figure 5 shows a 74 MHz image of the radio source Cygnus A imaged entirely with dual-frequency phase referencing and employing absolutely no self-calibration. This image demonstrates the power of phase referencing for removing the rapidly varying phase fluctuations introduced by the ionosphere and thereby restoring coherence to the data without any recourse to self-calibration. In this example phase referencing successfully increased the coherence time of the data from <1 m to >10 m. Such increased coherence times have significant implications for future imaging of weaker sources. Moreover, after phase referencing, self-calibration can be utilized with longer integration times to increase the dynamic range and otherwise improve the final image quality.

It should be noted that the phase referenced 74 MHz data will only be valid in a limited region defined by the direction to the 330 MHz field center. This so-called isoplanatic patch size (see also Sec. *4.3.2*), which depends on the spatial scales of ionospheric structure, has not been quantified, but is expected to be from one to several degrees across. As larger and more complex fields are imaged, its characteristics will become better defined.

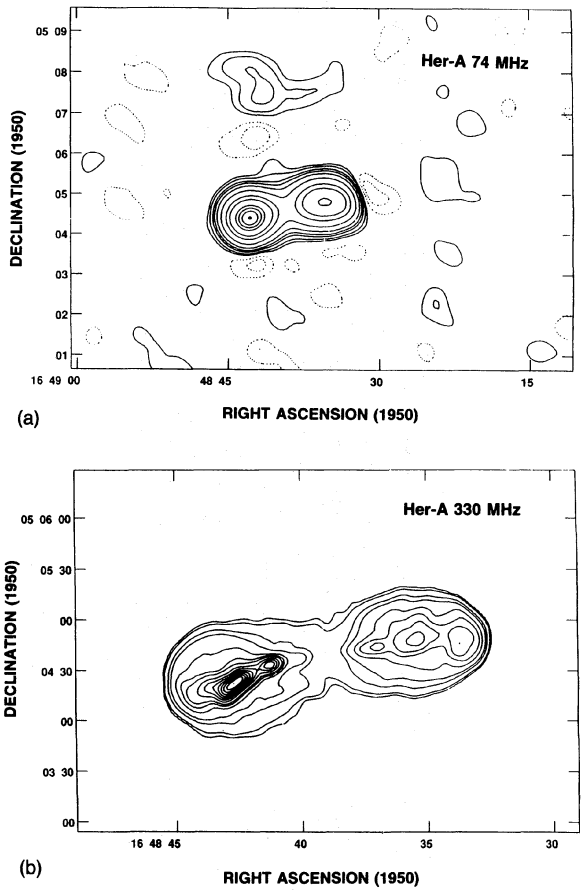

FIG. 8. Contour maps of the radio Galaxy Her A at 74 MHz (a) and 330 MHz (b). In (a) the peak brightness in the map is ~ 162 Jy beam^{-1}, the rms noise on the image is ~ 1 Jy beam^{-1}, and the angular resolution is $\sim 20''$. In (b) the peak brightness in the map is ~ 6.3 Jy beam^{-1}, the rms noise on the image is ~ 5 mJy beam^{-1}, and the angular resolution is $\sim 7''$. After further data are acquired, complete images will also be conducive to a spectral index analysis. Her A is known to be over-luminous for its morphology and it will be interesting to discover how it is aging.

4.3 Further Considerations

4.3.1 Ionospheric refraction

In practice we find an additional phase offset that arises when the dual frequency phase referencing technique is applied over long (>1 h) time scales. This is due to the fact that we assume the same source position for the two frequencies while there is actually a difference in the apparent position caused by ionospheric refraction. This introduces an offset between the 74 MHz phase and the scaled 330 MHz phase in addition to the instrumental offset. Figures 6(a) and 6(b) illustrate this offset, which over long time periods can drift at rates of ~ 1 rad h^{-1}. (An $\sim 1'$ difference between the 74 and 330 MHz, as would be expected from ionospheric refraction, easily explains this effect.) Over time scales of <1 h (and often for much longer periods) this offset remains fairly constant and merely introduces positional offsets in the phase referenced 74 MHz maps. There are various ways to deal with this problem; we normally solve it through self-calibration of the 74 MHz data.

4.3.2 The wide field imaging problem

A further important consideration for low frequency observations in general is the so-called 3-D imaging problem (Perley 1989; Perley & Cornwell 1991; Cornwell & Perley 1992). This arises because of the requirement, in principle, of a full three-dimensional (3-D) Fourier Transform to image properly the large field of view measured by a non-coplanar array at low frequencies. (Because the VLA is not a simple East–West array it can be approximated as a coplanar array only for single snapshot observations). This is a particular problem for the 74 MHz VLA system due to the unusually large primary beam and relatively long baselines involved. When it is ignored it leads to smearing as a function of distance from the field center for large sources and improper cleaning of sidelobes from strong (albeit compact) sources far from the field center.

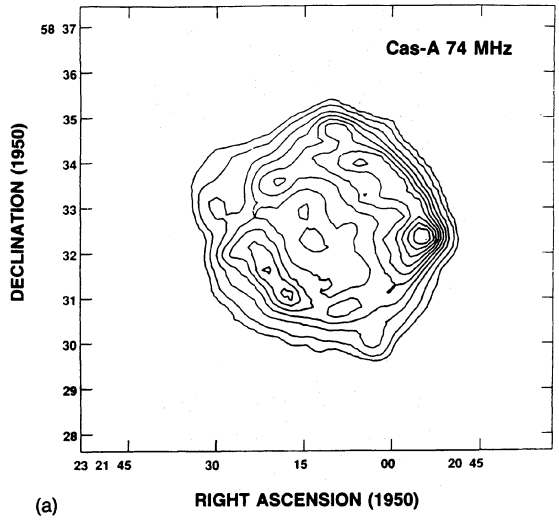

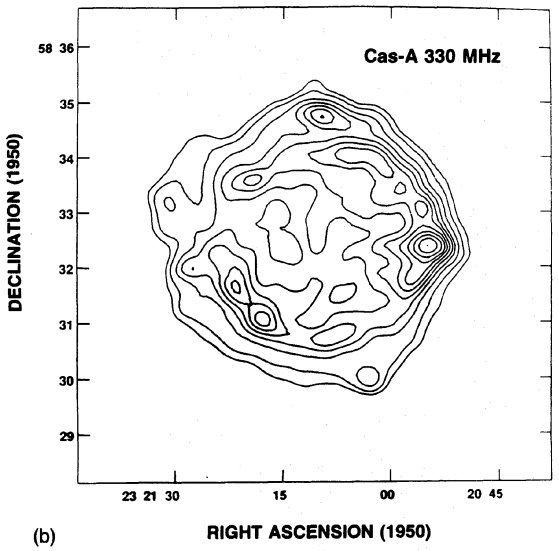

FIG. 9. Contour maps of the Galactic supernova remnant (SNR) Cas A at 74 MHz (a) and 330 MHz (b). For (a) the peak brightness in the map is $\sim$633 Jy beam^{-1}, the rms noise is $\sim$1 Jy beam^{-1}, and the angular resolution is $\sim$20″. For (b) the peak brightness in the map is $\sim$131 Jy beam^{-1}, the rms noise on the image is $\sim$125 mJy beam^{-1}, and the angular resolution is $\sim$20″. After additional short-spacing data is acquired, a spectral index map will be generated which will allow a search for spectral index variations across the source. Such variations across SNRs have been a source of controversy for many years, and definitive results have been hampered by the lack of images at low frequency with good angular resolution.

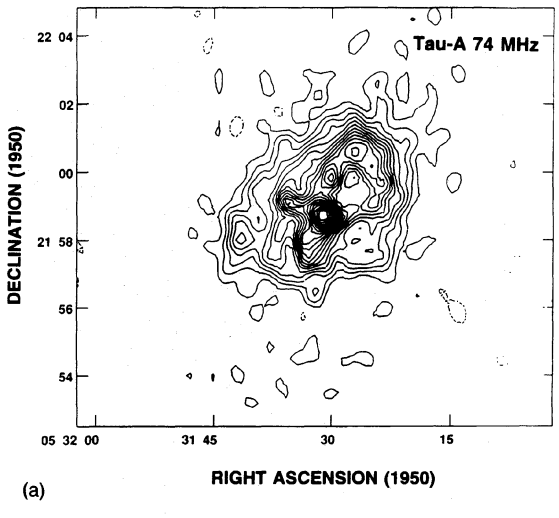

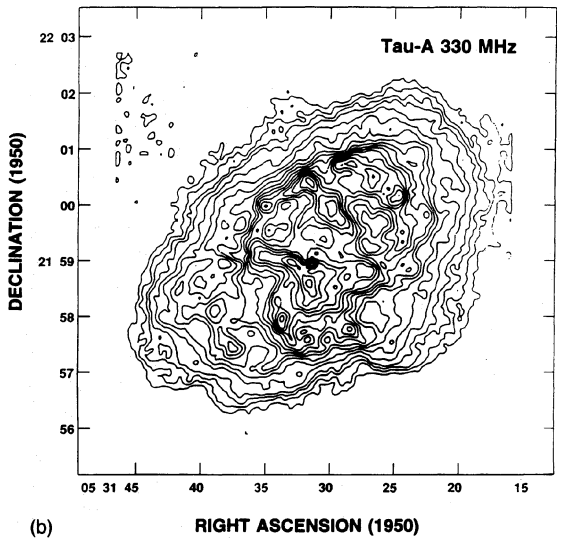

FIG. 10. Contour maps of Taurus A (Crab Nebula) at 74 MHz (a) and 330 MHz (b), respectively. In (a) the peak brightness in the map is $\sim$64 Jy beam^{-1}, the rms noise is $\sim$1 Jy beam^{-1}, and the angular resolution is $\sim$20″. In (b) the peak brightness in the map is $\sim$1 Jy beam^{-1}, the rms noise is $\sim$11 mJy beam^{-1}, and the angular resolution is $\sim$6″. The steep-spectrum Crab nebula pulsar is seen as a striking continuum feature on both maps.

While a practical solution to this problem is now available at 330 MHz (see Cornwell 1993, for a description of the 3-D polyhedron algorithm), further modifications are required before it can be applied to the 74 MHz data (Cornwell 1993). This is because at 74 MHz the isoplanatic patch size, while not yet well defined, is certainly smaller than the primary beam size. Furthermore, more baselines will be required since the number of unknowns (antennas times the number of isoplanatic patches within the primary beam) is much larger than at 330 MHz, where the isoplanatic patch size is larger than the primary beam size. When such wide-field imaging software does become available at 74 MHz, it will also greatly reduce the effects of confusion noted earlier, as has already been demonstrated at 330 MHz.

While the code required to correct for this effect is not yet on-line at the VLA, conventional 2-D Fourier imaging techniques have been adequate for the reduction of our initial data sets because: (1) Serious errors only arise when the product of the angular offset of the source in radians from the phase center multiplied by this same offset in synthesized beams exceeds unity. For A-array 74 MHz data this only occurs for sources larger than $\sim$90′ in diameter and most of our observed sources are smaller than

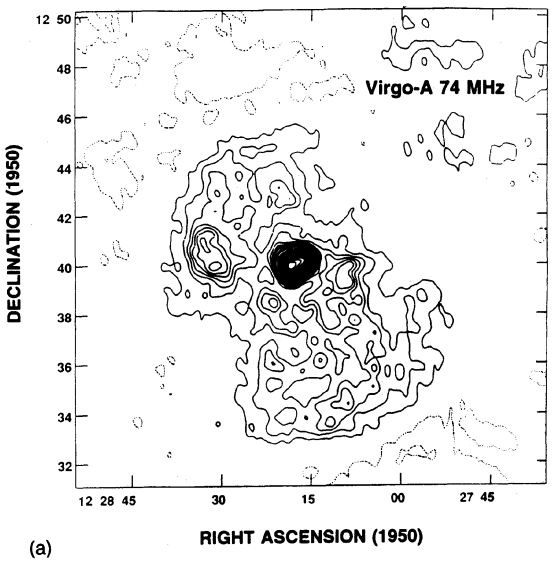

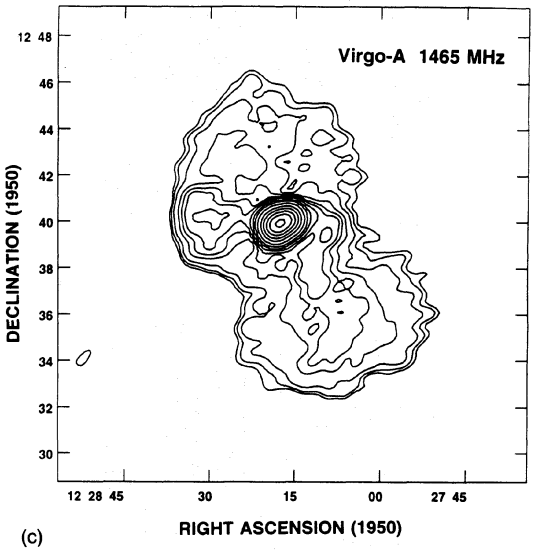

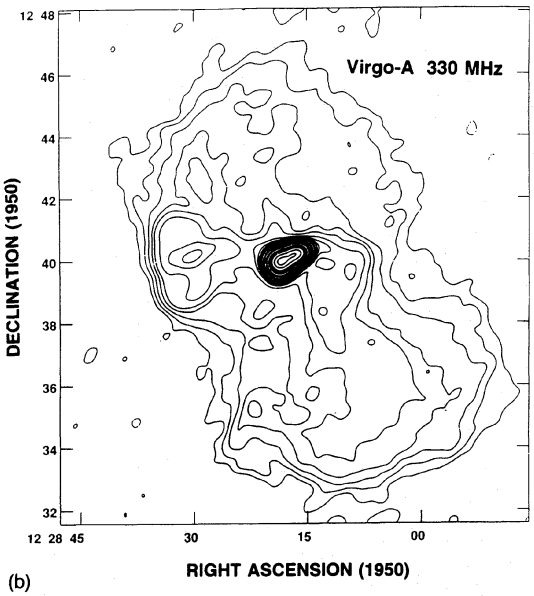

FIG. 11. (a) shows a 74 MHz image of the one-sided jet source Virgo A (M87). The peak brightness in the map is $\sim$253 Jy beam^{-1}, the rms noise is $\sim$1 Jy beam^{-1}, and the angular resolution is $\sim$20″. (b) shows our 330 MHz image which has a peak brightness of $\sim$76 Jy beam^{-1}, an rms noise level of $\sim$6 mJy beam^{-1}, and has been smoothed to an angular resolution comparable to that in (a). For comparison, (c) shows a VLA image of the source at 1465 MHz with a peak brightness of $\sim$83 Jy beam^{-1}, an rms noise level of $\sim$31 mJy beam^{-1}, and an angular resolution of $\sim$45″.

this. (2) These first sets of observed sources are sufficiently bright that the contribution to the noise level from sidelobes of unmodeled sources away from the field center (which would have been CLEANed incorrectly) is negligible. Obviously this will not be the case for future observations of large and weaker sources in more complex fields, and proper 3-D imaging will be required at both 330 and 74 MHz. This, however, is a daunting prospect at the lower frequency, since the background sources will occupy many different isoplanatic patches, requiring a sophisticated algorithm which will compute spatially variant phase corrections for each of the array's component antennas.

5. OBSERVATIONS

Our ongoing 74 MHz observations extend over two full VLA configuration cycles. This is needed because of the limited (u,v) coverage offered by only seven to eight elements. For most sources, the most important measurements are obtained in the A (maximum baselines $\sim$35 km) and B (maximum baselines $\sim$11 km) configurations, since only sources with structure larger than $\sim$10′–20′ require observations in more compact configurations. The observations were always conducted in a "two IF mode," with each IF measuring a single circularly polarized component (left in both cases) of the radiation at "*P* band" (327–333 MHz) and at "4 band" (73.8 MHz or $\lambda\sim$4 m wavelength), employing bandwidths of 3 MHz and 1.5 MHz, respectively. The data were taken in spectral line mode using 128 channels at 4 band and 64 channels at *P* band. As described in Sec. 3 this was sometimes necessary in order to remove harmonics of internally generated interference. After excision of the interfering channels, the data were then converted to a standard continuum data base for further reduction.

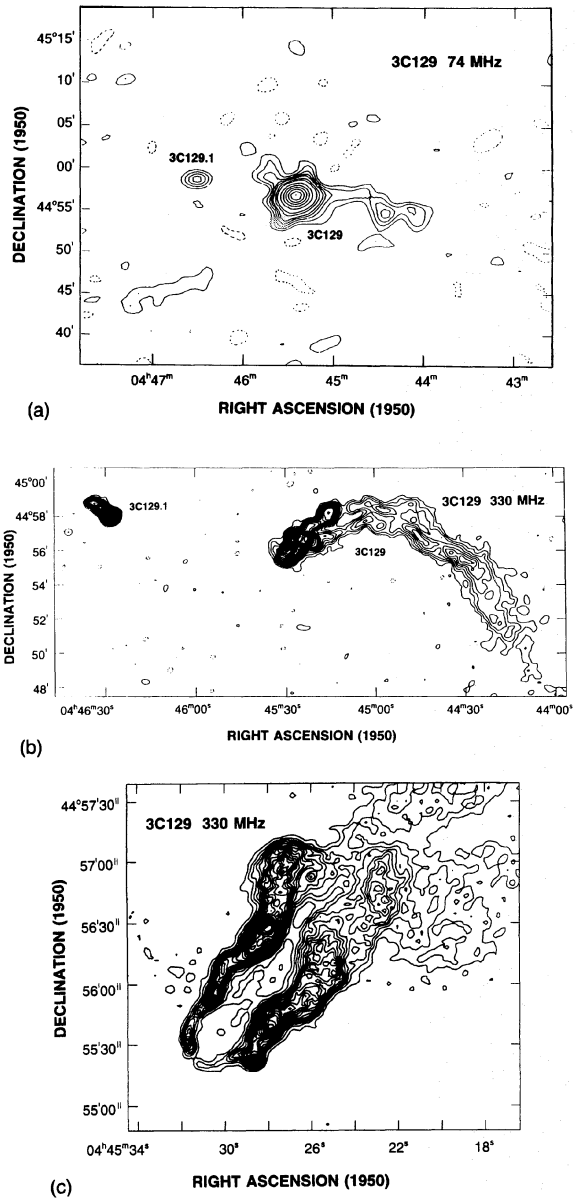

FIG. 12. Contour maps of 3C129 at 74 MHz (a) and at 330 MHz (b) and (c). On (a), the peak brightness in the map is ~ 26 Jy beam^{-1}, the rms noise is ~ 700 mJy beam^{-1}, and the angular resolution is $\sim 1'$. On (b), the peak brightness in the map is ~ 790 mJy beam^{-1}, the rms noise is ~ 5 mJy noise^{-1}, and the angular resolution is $\sim 20''$. On (c) (a close-up of the "head") the peak brightness is ~ 75 mJy beam^{-1}, the rms noise is ~ 3 mJy beam^{-1}, and the angular resolution is $\sim 6''$. 3C129 is a strong and very extended ($> 20'$) head–tail radio Galaxy, making it an excellent candidate for observation at high resolution at long wavelengths. It exhibits spectral index variations along its tail and a good 74 MHz map is needed to nail down these variations. Further ongoing observations are being obtained at 74 MHz to establish the sensitivity and dynamic range required for useful scientific analysis. For weaker sources like this (brightness < 5 Jy beam^{-1}) such observations will be obtainable in much shorter periods of time when the system expands as planned.

6. FIRST MAPS

Figures 7–12 show preliminary maps of several prominent radio sources imaged using the 74 MHz receiving system. For these exceptional sources, self-calibration without resorting to phase referencing was generally sufficient for generating images because of their high flux densities, although phase referencing, described in Sec. *4.2*, was sometimes applied to the data in order to increase the coherence time. Other than that, the data were reduced, Fourier transformed, and CLEANed in the standard manner.

Ongoing reduction of these and other observations is very encouraging and is providing low frequency images with the unprecedented resolution of $< 30''$ at 74 MHz. These images hold the prospect of generating spectral index maps which can address several fundamental scientific issues, although further data are required before meaningful conclusions can be drawn. We defer detailed discussion of these to future papers after our ongoing observations are completed. We note also that the 330 MHz images (with $\sim 6''$ resolution) obtained as a matter of course during these observations are often the best images available at that frequency, and a few of those images are also shown. The noise levels on the 74 MHz images at or below the 1 Jy beam^{-1} level brings many other sources within range of the new observing system (i.e., a good fraction of 3C sources). The accompanying figure captions give brief descriptions of each source. Please note that while peak brightness temperatures and noise levels are listed in the captions for reference, these preliminary images should not be used for absolute measurements. While the relative brightness temperatures are valid, absolute flux density calibration has not been rigorously applied to these data. This is of little consequence to these first observations since nearly all of these sources have well determined *integrated* flux densities at low frequencies.

7. CONCLUSIONS AND FUTURE PROSPECTS

We have described a new low frequency observing system at the VLA that makes use of simple dipoles mounted on a subset of the VLA antennas, utilizes the standard waveguide transmission system, VLA correlator, and existing computer network. The system is capable of imaging sources at 74 MHz with 20″ resolution, thereby opening a new window for long baseline (> 5 km), high resolution, low frequency interferometry which can be conducted from the Earth's surface. Preliminary maps of several radio sources imaged with the new system have been presented. This work demonstrates the power of several recently developed imaging techniques to overcome difficulties, most notably those imposed by the Earth's ionosphere, which have restricted previous low frequency synthesis instruments to much shorter baselines.

For strong sources, we find that self-calibration is adequate for removing the effects of the ionosphere. The current system works well for imaging sources with correlated flux densities per baseline of $\geqslant$5–10 Jy, corresponding to sources with typical integrated flux densities of $\geqslant$200–500 Jy. This is because: (1) amplitude and phase errors due to contributions from unmodeled confusing sources are negligible; and (2) there is sufficient S/N on short time scales to allow for robust self-calibration. For weaker sources, we

have developed a method of dual frequency ionospheric phase referencing for removing the effects of ionospheric phase variations. This technique makes use of the VLA's ability to obtain data simultaneously at two frequencies. This ionospheric phase referencing technique is applicable to any future long baseline, low frequency system which will allow dual frequency operation.

Limitations in sensitivity and (u,v) coverage are caused by the fact that only eight antennas are equipped for 74 MHz operation. If all the VLA antennas were equipped for this frequency, the additional (u,v) coverage would both mitigate the effects of confusion and, by providing new closure phase information, improve the performance of the self-calibration algorithm. Based on the noise levels in our preliminary maps, we project that a 12 h observation with a 27 antenna 74/330 MHz system could achieve noise levels of below 100 mJy beam^{-1} at 74 MHz. All of the 3C and 4C sources should then be observable.

We note that there are no serious restrictions (other than cost) to attaching 74 MHz feeds to a subset of NRAO's VLBA antennas in order to further increase the angular resolution (Napier 1992). In fact, the design of the VLBA dishes should provide for improved aperture efficiency relative to the VLA dishes. As implied long ago from experience gained in low frequency VLBI (Carr *et al.* 1970; Erickson *et al.* 1972; Clark *et al.* 1975; Hartas *et al.* 1983) limits on the highest useful angular resolution will be set by nature (e.g., from limited brightness temperatures due to self-absorption in compact sources and from resolution limits imposed by interstellar and interplanetary "seeing"[4]) and not by limits in technology.

Finally, when resources permit, we suggest that the original proposal for a stand-alone system as proposed by Perley & Erickson (1984) should be implemented at an even lower frequency to complement the 74 MHz VLA system. In this frequency range it is relatively cheap and easy to build simple arrays that would have more gain and lower sidelobe levels than the VLA dishes. Such a system would also be excellent for solar and ionospheric work as well as for cosmic source work. Ionospheric and solar work require either long or full-time observing sessions for which it would not be practical to tie up the VLA.

We acknowledge the contribution of many NRAO staff members without whose help the development of this unique system would not have been possible. These especially include D. Bagri, B. Clark, T. Cornwell, J. Pettinson, and K. Sowinski. Basic research in Radio Interferometry at the Naval Research Laboratory is supported by the Office of Naval Research through funding document number N00014-93-WX-35012, under NRL work unit 2567.

[4]Estimates of the limiting resolution imposed by interstellar scintillation near 74 MHz are ~5″ at the Galactic equator and ~0.2″ near the Galactic poles (Baldwin 1984). See Spangler & Armstrong (1990) for a discussion of the effects of interplanetary scintillation at low frequencies.

REFERENCES

Baars, J. W. M., Genzel, R., Pauliny-Toth, I. I. K., & Witzel, A. 1977, A&A, 61, 99
Baldwin, J. E. 1984, in *Indirect Imaging*, edited by J. A. Roberts (Cambridge University Press, Cambridge), p. 11
Carr, T. D., Lynch, M. A., Paul, M. P., Brown, G. W., May, J., Six, N. F., Robinson, V. M., & Block, W. F. 1970, Radio Science, 5, 1223
Clark, T. A., Erickson, W. C., Hutton, L. K., Resch, G. M., and Vandenberg, N. R. 1975, AJ, 80, 923
Cornwell, T. J. 1993, VLA Scientific Memorandum #164
Cornwell, T. J. 1993, private communication
Cornwell, T. J. and Perley, R. A. 1992, Astron. Astrophys. 261 353
1975, Astron. J., 80, 923
Dreher, J. W. and Feigelson, E. 1984, Nature, 308, 43
Dwarakanath, K. S. and Udaya Shankar, N. 1990, J. Astrophys. Astron., 11, 323
Erickson, W. C., Kuiper, T. B. H., Clark, T. A., Knowles, S. H., & Broderick, J. J. 1972, ApJ, 177, 101
Hartas, J. S., Rees, W. G., Scott, P. F., & Duffett-Smith, P. J., 1983, MNRAS, 205, 625
Haslam, C. G. T., Salter, C. J., Stoffel, H., & Wilson, W. E. 1982, 47, 1
Jacobson, A. R., & Erickson, W. C. 1992a, A&A, 257, 401
Jacobson, A. R., & Erickson, W. C. 1992b, Planet. Space. Sci., 40, 447
Kassim, N. E., & Weiler, K. W., Eds. 1990, Low Frequency Astrophysics from Space, Springer-Verlag Lecture Notes in Physics, 362 (Springer, Heidelberg)
Landecker, T. L., & Wielebinski, R. 1970, AuJPA, 16, 1
Napier, P. 1992, private communication
Pearson, T. J., & Readhead, A. C. S. 1984, ARA&A, 22, 97
Perley, R. A. 1989, in Synthesis Imaging in Radio Astronomy, ASP Conference Series, edited by R. A. Perley, F. R. Schwab, and A. H. Bridle (ASP, Provo) Vol. 6, 259
Perley, R. A., & Cornwell, T. J. 1991, in Radio Interferometry: Theory, Techniques, and Applications, ASP Conference Series, edited by T. J. Cornwell and R. A. Perley (ASP, Provo), Vol. 19, p. 184
Perley, R. A., & Erickson, W. C. 1984, NRAO Scientific Memorandum #146
Spangler, S. R., & Armstrong, J. W. 1990, in Low Frequency Astrophysics from Space, Lecture Notes in Physics, edited by N. E. Kassim and K. W. Weiler (Springer, Heidelberg), Vol. 362, p. 155
Swarup, G. 1993, private communication
Yates, K. W. 1968, AuJPh, 21, 167